

# Quinone ( $Q_B$ ) Reduction by B-Branch Electron Transfer in Mutant Bacterial Reaction Centers from *Rhodobacter sphaeroides*: Quantum Efficiency and X-ray Structure<sup>†,‡</sup>

M. L. Paddock,\* C. Chang, Q. Xu,<sup>§</sup> E. C. Abresch, H. L. Axelrod,<sup>||</sup> G. Feher, and M. Y. Okamura

Department of Physics, University of California, San Diego, 9500 Gilman Drive, La Jolla, California 92093

Received November 19, 2004; Revised Manuscript Received March 10, 2005

**ABSTRACT:** The photosynthetic reaction center (RC) from purple bacteria converts light into chemical energy. Although the RC shows two nearly structurally symmetric branches, A and B, light-induced electron transfer in the native RC occurs almost exclusively along the A-branch to a primary quinone electron acceptor  $Q_A$ . Subsequent electron and proton transfer to a mobile quinone molecule  $Q_B$  converts it to a quinol,  $Q_BH_2$ . We report the construction and characterization of a series of mutants in *Rhodobacter sphaeroides* designed to reduce  $Q_B$  via the B-branch. The quantum efficiency to  $Q_B$  via the B-branch  $\Phi_B$  ranged from 0.4% in an RC containing the single mutation Ala-M260  $\rightarrow$  Trp to 5% in a quintuple mutant which includes in addition three mutations to inhibit transfer along the A-branch (Gly-M203  $\rightarrow$  Asp, Tyr-M210  $\rightarrow$  Phe, Leu-M214  $\rightarrow$  His) and one to promote transfer along the B-branch (Phe-L181  $\rightarrow$  Tyr). Comparing the value of 0.4% for  $\Phi_B$  obtained in the AW(M260) mutant, which lacks  $Q_A$ , to the 100% quantum efficiency for  $\Phi_A$  along the A-branch in the native RC, we obtain a ratio for A-branch to B-branch electron transfer of 250:1. We determined the structure of the most effective (quintuple) mutant RC at 2.25 Å ( $R$ -factor = 19.6%). The  $Q_A$  site did not contain a quinone but was occupied by the side chain of Trp-M260 and a  $Cl^-$ . In this structure a nonfunctional quinone was found to occupy a new site near M258 and M268. The implications of this work to trap intermediate states are discussed.

Electron transfer is a fundamental step in the conversion of light into chemical energy in photosynthetic organisms. One of the most studied photosynthetic species is the purple non-sulfur bacterium *Rhodobacter (Rb.) sphaeroides* (e.g., refs 1 and 2). The energy conversion process begins in a membrane-bound pigment protein complex called the reaction center (RC)<sup>1</sup> with photoexcitation of the primary donor, a bacteriochlorophyll dimer (D), followed by electron transfer. Although the RC structure shows two nearly symmetric pigment branches, called A and B, electron transfer proceeds almost exclusively along the A-branch (Figure 1) with a quantum efficiency near 100% via a bacteriopheophytin ( $H_A$ ) to the tightly bound primary quinone,  $Q_A$ . Subsequent electron transfer occurs from  $Q_A^{\cdot-}$  to

<sup>†</sup> This work has been supported by the National Institutes of Health (Grants GM-13191 and GM 41637).

<sup>‡</sup> PDB accession code 1YF6.

\* To whom correspondence should be addressed. Phone: (858) 534-2504. Fax: (858) 822-0007. E-mail: mpaddock@physics.ucsd.edu.

<sup>§</sup> Current affiliation: Cardiovascular Research Institute, University of California, San Francisco, San Francisco, CA 94143.

<sup>||</sup> Current affiliation: Joint Center for Structural Genomics, Stanford Synchrotron Radiation Laboratory, Menlo Park, CA 94025.

<sup>1</sup> Abbreviations: RC, reaction center; D, primary donor, dimer of bacteriochlorophylls;  $B_A$  and  $B_B$ , bacteriochlorophyll A-branch and B-branch, respectively;  $H_A$  and  $H_B$ , bacteriopheophytin A-branch and B-branch, respectively;  $\beta$ , non-native bacteriochlorophyll;  $Q_A$ , primary quinone electron acceptor;  $Q_B$ , secondary quinone electron acceptor;  $k_{AB}^{(1)}$ , rate of first electron transfer from  $Q_A^{\cdot-}$  to  $Q_B$ ;  $k_{AB}^{(2)}$ , rate of second electron transfer from  $Q_A^{\cdot-}$  to  $Q_B$ ;  $\Phi_A$  and  $\Phi_B$ , quantum efficiency for electron transfer along the A-branch and B-branch, respectively.

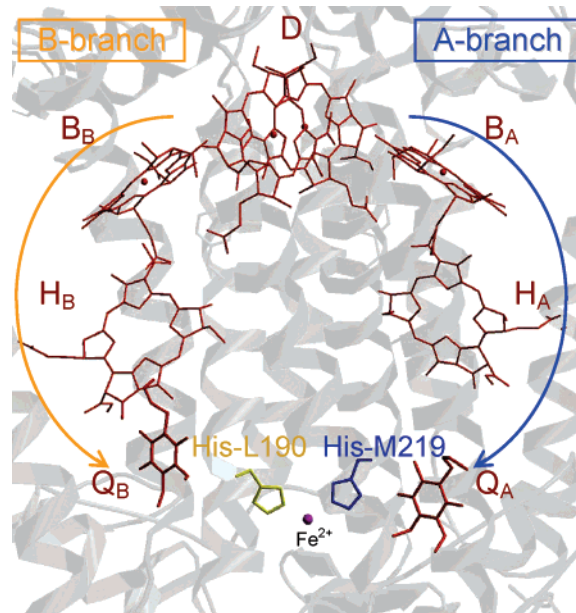


FIGURE 1: Structure of the RC protein backbone (gray) and cofactors (red). D is the primary donor, a bacteriochlorophyll dimer,  $B_A$  and  $B_B$  are bacteriochlorophylls,  $H_A$  and  $H_B$  are bacteriopheophytins, and  $Q_A$  and  $Q_B$  are quinone molecules; the subscripts A and B refer to which branch of the RC the cofactor binds. The  $Fe^{2+}$  ligands His-L190 (yellow) and His-M219 (blue), which stabilize the semiquinone states, are shown. Light-induced electron transfer proceeds predominantly along the A-branch in the native RC. We focus in this work on electron transfer along the B-branch (yellow arrow). (PDB entry 1AII; ref 15.)

the secondary quinone,  $Q_B$  (3–6). Following reduction of  $D^{+}$ , a second electron is transferred through the A-branch to  $Q_B^{-}$  (7, 8). The light-induced electron transfer is coupled to proton uptake (see, e.g., ref 9), resulting in the formation of a quinol molecule,  $Q_BH_2$ , at the  $Q_B$  site (eq 1) (reviewed



in refs 2 and 10–12). Equation 1 proceeds via two sequential proton-coupled electron transfer steps, each of which involves intermediate state(s) (6, 13) that are thermally activated (i.e., higher in energy than the initial and final states) (4, 14). This makes it difficult to observe the intermediate states involved in the electron transfer processes. To overcome this difficulty, we modified the RC by site-directed mutagenesis to enhance electron transfer through the normally inactive B-branch. Electron transfer along the B-branch to  $Q_B$  occurs via a bacteriopheophytin,  $H_B$  (Figure 1), with a much larger electron transfer driving force (16) than from  $Q_A^{-}$ . Consequently, intermediate states that are involved in the electron transfer processes become thermodynamically more accessible.

Over the last 20 years much work has been done on B-branch electron transfer in mutant RCs designed to enhance B-branch electron transfer (4, 16–36). In this work, we focused on four mutations that had been shown to increase the quantum efficiency along the B-branch (mostly in *Rb. capsulatus*): three to inhibit A-branch electron transfer and one to facilitate B-branch electron transfer. One of the three A-branch mutations was Leu-M214  $\rightarrow$  His [LH(M214)], which results in the creation of a bacteriochlorophyll, called  $\beta_A$ , at the  $H_A$  site (18). A second was Gly-M203  $\rightarrow$  Asp [GD(M203)], which introduces an Asp near  $B_A$  (20, 31, 37). A third was Tyr-M210  $\rightarrow$  Phe [YF(M210)], located near  $B_A$  (Figure 1) (29, 30). The mutation designed to increase B-branch electron transfer was Phe-L181  $\rightarrow$  Tyr [FY(L181)], located near  $B_B$  (29, 30). We combined these mutations with a mutation that eliminates the native electron transfer pathway by removing  $Q_A$ ; this was accomplished by replacing Ala-M260 by Trp [AW(M260)] (38). The Trp occupies part of the  $Q_A$  headgroup binding region, thereby preventing the binding of a quinone ring system (39).

Most of the work on the above-mentioned mutations had been previously performed in the related bacterium *Rhodospirillum rubrum*. The GD(M201)/LH(M212) (*Rb. capsulatus* numbering, which is two less than that in *Rb. sphaeroides*) double mutant increased the quantum yield to 15% for B-branch electron transfer to  $H_B$  (20, 22). Introducing these same mutations in *Rb. sphaeroides* increased B-branch quantum efficiency to  $H_B$  to 7%, i.e.,  $\sim$ 2-fold smaller than in *Rb. capsulatus* (29). The YF(M208)/FY(L181) double mutant in *Rb. capsulatus* had an increased quantum efficiency of 30% for B-branch electron transfer to  $H_B$  (27). Although their effects in *Rb. sphaeroides* have not been established, we estimated that their introduction would increase the B-branch quantum efficiency to 15% (one-half of that reported for *Rb. capsulatus*). Our goal was to obtain a mutant RC from *Rb. sphaeroides* with as large a B-branch quantum efficiency as possible. The quantum efficiency of electron transfer to  $Q_B$  may be smaller than that to  $H_B$  by an amount that depends on the efficiency of electron transfer from  $H_B^{-}$  to  $Q_B$ , which has been reported

to be between 20% and 80% in *Rb. capsulatus* mutant RCs (16).

In this study, we constructed a series of mutant RCs from *Rb. sphaeroides* in which the mutations discussed above were added sequentially, resulting in a series of B-branch mutant RCs containing up to five mutations; only two of these constructs had previously been reported in *Rb. sphaeroides* (31, 32, 34). Our goal was to incorporate all of the mutations into a single RC (quintuple mutant RC) to maximize the quantum efficiency in *Rb. sphaeroides* for the net electron transfer to  $Q_B$  via the B-branch. We describe the method used to determine the B-branch electron transfer quantum efficiency to  $Q_B$  in the series of mutant RCs. From these values the ratio of A-branch to B-branch electron transfer in the native RC was determined. To aid in the interpretation of the results obtained on the mutant RCs, the crystal structure of the quintuple mutant was determined. The success of the constructs to generate  $Q_B^{-}$  via the B-branch opens the way to investigate intermediate states involved in the reduction of  $Q_B$ . A preliminary account of this work has been presented (40, 41).

## MATERIALS AND METHODS

**Design and Construction of Mutant RCs.** The mutations were incorporated into the *puf* operon as previously described (42). The oligonucleotides used in constructing the mutant genes contained approximately three to four codons of flanking DNA on both sides of the nucleic acid change(s). A series of five oligonucleotides and their complements were synthesized (IDT, Coralville, IA) with the following codon changes: GCC  $\rightarrow$  TGG (Ala-M260  $\rightarrow$  Trp), CTG  $\rightarrow$  CAC (Leu-M214  $\rightarrow$  His), TAC  $\rightarrow$  TTC (Tyr-M210  $\rightarrow$  Phe), GGT  $\rightarrow$  GAC (Gly-M203  $\rightarrow$  Asp), and TTC  $\rightarrow$  TAC (Phe-L181  $\rightarrow$  Tyr). The desired mutations were incorporated into the gene sequence using the QuikChange mutagenesis system (Stratagene, Cedar Creek, TX) and a Perkin-Elmer PCR system. The first step was the introduction of the AW(M260) mutation, which is present in all mutant RCs discussed in this work. Subsequently, mutations were sequentially introduced into the template creating two double mutants [GD(M203)/AW(M260), LH(M214)/AW(M260)], followed by three triple mutants [GD(M203)/LH(M214)/AW(M260), FY(L181)/LH(M214)/AW(M260), YF(M210)/LH(M214)/AW(M260)], one quadruple mutant [FY(L181)/YF(M210)/LH(M214)/AW(M260)], and finally a quintuple mutant [FY(L181)/GD(M203)/YF(M210)/LH(M214)/AW(M260)]. All mutations were verified by sequence analysis performed at the DNA Sequencing Shared Resource, UCSD Cancer Center. The final modified fragments were incorporated into the pRKMUT expression vehicle; the proper constructs were confirmed by restriction enzyme digests and transferred into the deletion strain  $\Delta$ LM1.1 via *Escherichia coli* S17-1 as described (42). *Rb. sphaeroides* cells were selected for resistance to tetracycline, indicating the successful transfer of the pRK plasmid. These complemented deletion strains were used for photosynthetic growth tests and RC isolation.

**Growth of Mutant Bacteria.** The complemented deletion strains were grown in two ways: semiaerobic in the dark for RC production and isolation and anaerobic in the light for photosynthetic tests as described by Paddock et al. (42). The former set of conditions results in RC production but

does not require a functional RC for growth. In contrast, a functional RC is required for photosynthetic growth under anaerobic conditions.

**Isolation and Purification of RCs.** The RC protein was isolated from semiaerobically grown cells as described (43). The optical absorbance ratio  $A^{280}/A^{802}$  was  $\leq 1.3$  for all RCs used in the kinetic studies. For crystallization of the quintuple mutant RC the ratio was 0.95; this is smaller than that for the native RC due to the LH(M214) mutation, which results in the introduction of a new bacteriochlorophyll,  $\beta_A$ , which increases the 802 nm absorption (18). The secondary quinone  $Q_B$  was lost during purification and was reconstituted by adding  $\sim 3$ -fold UQ<sub>10</sub> in 1% LDAO prior to a 1 day dialysis against TLE (10 mM Tris-HCl, pH 8, 0.025% LDAO, 0.1 mM EDTA) followed by a 1 day dialysis in TMK (2 mM Tris-HCl, pH 8, 0.04%  $\beta$ -D-maltoside, 5 mM KCl). Prior to measurements  $\sim 5 \mu\text{M}$  ferricyanide was added to the samples.

**Kinetic Measurements.** Kinetic measurements were performed on a home-built spectrometer (4) using a Nd:YAG laser (Opotek, Carlsbad, CA) for actinic excitation (40 mJ per pulse,  $\sim 5$  ns half-width). Kinetic traces were recorded on a LeCroy oscilloscope and then transferred to a PC for analysis.

**Determination of Quantum Efficiency  $\Phi_B$  Using a Train of Laser Flashes.** The quantum efficiency of electron transfer to  $Q_B$ ,  $\Phi_B$ , was obtained from the rate of charge separation for a given frequency of saturating laser flashes ( $n$ ). The basic equation is



where  $DQ_B$  is the RC in the ground state,  $D^+ \cdot Q_B^-$  is the RC in the excited charge-separated state, and  $k_{ex}$  and  $k_{BD}$  are the excitation and recombination rate constants, respectively. As the sample is excited with light (starting at time  $t = 0$ ), the  $D^+ \cdot Q_B^-$  state accumulates until the rate of recombination competes with the rate of excitation. When these two rates are equal, a steady-state population is reached (i.e., no further changes in absorbance are observed). The differential equation that describes this process is

$$d[DQ_B]/dt = -d[D^+ \cdot Q_B^-]/dt = -k_{ex}[DQ_B] + k_{BD}[D^+ \cdot Q_B^-] \quad (3)$$

Since the flashes are saturating, the excitation rate is controlled by  $n$ . Replacing the excitation rate constant  $k_{ex}$  with  $n\Phi_B$ , where  $n$  is the flash frequency and  $\Phi_B$  is the quantum efficiency,  $[D^+ \cdot Q_B^-]$  with  $\Delta A^{865}/\Delta\epsilon$ , where  $\Delta\epsilon$  is the differential extinction coefficient for a 1 cm path length, and total [RC] with  $\Delta A^{865}_{max}/\Delta\epsilon$ , obtained upon excitation with saturating CW light (0.5 W/cm<sup>2</sup>), yields the solution (44):

$$\Delta A^{865}(t) = \Delta A^{865}_{max} \frac{n\Phi_B}{n\Phi_B + k_{BD}} \{1 - \exp[-(n\Phi_B + k_{BD})t]\} \quad (4)$$

which is independent of the extinction coefficient. The term outside the parentheses represents the steady-state fraction which is a function of the formation and decay rate constants, and the term in parentheses represents the rate at which

steady state is achieved. Note that the expression, which is independent of the extinction coefficient, can be applied to all RCs independent of the cofactor composition.

When the illumination is stopped ( $t' = 0$ ), the sample decays back to the initial ground state with a decay constant  $k_{BD}$  given by

$$\Delta A^{865}(t') = \Delta A^{865}(t'=0) \{ \exp[-(k_{BD})t'] \} \quad (5)$$

The advantage of this method is that  $n$  is controlled by the laser flash frequency and  $\Delta A^{865}$  and  $k_{BD}$  are independently measured, leaving  $\Phi_B$  as the only free parameter. The value of  $k_{BD}$  was determined from the exponential recovery following excitation (eq 5).

**Crystallization and X-ray Data Collection.** Crystals of the quintuple mutant RC in the trigonal form (space group  $P3_1-21$ ) (45, 46) were obtained by vapor diffusion at 19 °C in 20  $\mu\text{L}$  sitting drops with a 1 mL reservoir in Cryschem type plates (Charles Supper Co., Natick, MA). One day prior to freezing and X-ray data collection, an  $\sim 3$ – $5$ -fold excess of UQ<sub>4</sub> was added to the solution containing the crystals. X-ray diffraction data were collected at a wavelength of 1.00 Å on crystals cooled to  $\sim 100$  K at the Advanced Light Source (ALS) beamline 5.0.1. The crystallization conditions and the flash-freeze protocol have been described previously (47; condition 3 in Table 3). The diffraction data were integrated with MOSFLM (48) software packages and scaled with the CCP4 SCALA (Collaborative Computational Project, 1994) program.

**X-ray Structure Determination.** The 1.80 Å resolution structure of the RC double mutant DN(L213)/RC(M233) (PDB accession code 1RZH) (47) was used as a starting model for the refinement of the structure of the quintuple mutant RC. Water molecules, detergent molecules, lipids, other small molecules (e.g., phosphate), and both quinone molecules were omitted from the starting model. In the later stages of refinement, bound water molecules were added into  $F_o - F_c$  difference electron density peaks that were  $> 3\sigma$  above the background level of the map and within 4 Å of potential hydrogen bond donors and acceptors.  $Q_B$  was added at this stage, and residues near the  $Q_A$  site were manually adjusted. Rigid body, positional, simulated annealing, and isotropic temperature factor refinements were carried out with the CNS package (49). Between each round of refinement,  $2F_o - F_c$  and  $F_o - F_c$  electron density maps were calculated using the CNS package. The maps were inspected, and the models were manually revised using the computer graphics program XtalView (50).

## RESULTS

**Isolation and Spectral Characterization of Mutant RCs.** All mutant RCs included the AW(M260) mutation which eliminates the native electron transfer pathway through  $Q_A$  by displacing the bound quinone molecule (38). Additional mutations designed to increase the quantum efficiency of B-branch electron transfer to  $Q_B$  were introduced. The series consisted of LH(M214) (18), GD(M203) (20, 31, 37), YF-(M210), and FY(L181) (29, 30). The mutations were incorporated as described in Materials and Methods and confirmed by sequence analysis. Active RC proteins were isolated as described in Materials and Methods. Optical spectroscopy was used to identify the RC and determine its

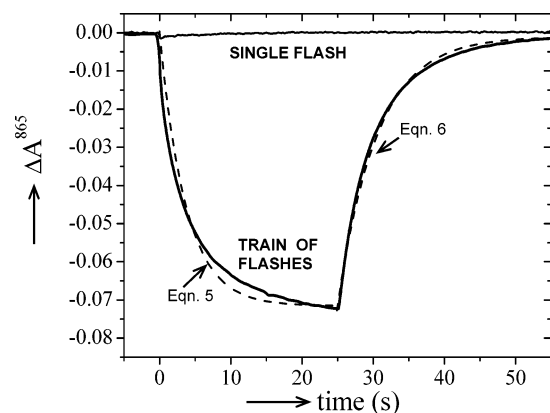


FIGURE 2: Generation of the charge-separated state  $D^+Q_B^-$  in the AW(M260) mutant RC monitored by the optical change  $\Delta A^{865}$ . At time  $t = 0$ , excitation of the sample is initiated by either a single laser flash (solid line) or a train of flashes (dashed line) from a Nd:YAG laser running at 10 Hz. At  $t \sim 25$  s, the train of laser flashes is stopped, and the charge recombination restores the RC to the ground state. The train of flashes increases the observed signal, allowing for a more reliable determination of the quantum efficiency  $\Phi_B$ . The decrease of the absorbance during illumination was modeled using eq 4 with  $\Phi_B = 0.3\%$  (dotted) and the increase (recovery) after termination of the illumination by eq 5 with  $k_{BD} = 0.17 \text{ s}^{-1}$  (dotted line). (Conditions:  $3 \mu\text{M}$  RC,  $2 \text{ mM}$  Tris-HCl, pH 8,  $0.04\%$   $\beta$ -D-maltoside,  $5 \text{ mM}$  KCl).

purity. In mutant RCs with the LH(M214) mutation, the optical spectrum showed an increase in the  $A^{800}$  absorption and a concomitant decrease in  $A^{760}$  compared to the native or other mutant RCs, confirming the transformation of the bacteriopheophytin,  $H_A$ , to a bacteriochlorophyll,  $\beta_A$  (18).

**Photosynthetic Growth.** The bacteria harboring the mutant RCs were tested for their ability to grow photosynthetically. None of the constructs, all of which lacked  $Q_A$ , could grow photosynthetically. However, three revertants were isolated. All of these had a mutation at the  $Q_A$  site, Trp-M260  $\rightarrow$  Cys (one case) or to Gly (two cases), which restored  $Q_A$  binding as shown by the  $\sim 100$  ms recombination time characteristic of the  $D^+Q_A^-$  state and its insensitivity to  $Q_B$  site inhibitors. The suppressor mutations are the same as those reported for the photosynthetic revertants of the single AW(M260) mutant in *Rb. sphaeroides* (51).

**Charge Separation in the Mutant RCs.** The purified mutant RCs lacked  $Q_B$  as shown by the lack of the charge-separated state  $D^+Q_B^-$  upon excitation with saturating laser flashes (not shown). However, upon addition of 2–3 equiv of ubiquinone a relatively long-lived ( $\tau \sim 7$  s) charge-separated state was produced. This state could be photoaccumulated with extended light exposure using either continuous illumination or a train of laser flashes at a frequency greater than the recombination rate, i.e., at a flash frequency greater than  $\sim 0.2$  Hz (see, e.g., Figure 2). This charge-separated state involved the formation of  $Q_B^-$  as was shown by the elimination of the absorbance change upon the addition of known  $Q_B$  inhibitors such as terbutryne and stigmatellin. Furthermore, the recombination rate of the inhibitor-sensitive phase was  $\sim 0.17 \text{ s}^{-1}$  ( $\pm 10\%$ ), which is the same as that determined for direct recombination from  $Q_B^-$  to  $D^+$  (52–54).

Upon addition of higher concentrations of ubiquinone, an inhibitor-insensitive phase with a time constant longer than 7 s was observed. Its amplitude and rate were proportional

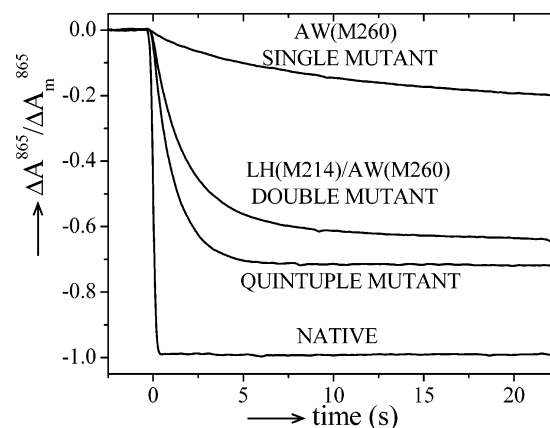


FIGURE 3: Comparison of the generation of the charge-separated state  $D^+Q_B^-$  in the native and three mutant RCs by a train of flashes as described in Figure 2. The traces are normalized to the maximum absorbance change at 865 nm, i.e.,  $\Delta A^{865}(t)/\Delta A^{865}_{\text{max}}$ . The native RC shows the expected behavior for a high quantum efficiency process ( $\Phi_A = 100\%$ ). In the mutant RCs, the electron transfer through the A-branch to  $Q_B$  is blocked (34, 35). The smaller quantum efficiency through the B-branch  $\Phi_B$  is seen by the slower rate at which the charge separation is generated as well as by the smaller steady-state level. The values for  $\Phi_B$  were obtained by fitting the data to eq 4 and are summarized in Table 1. (Conditions: same as in Figure 2.)

to the ubiquinone concentration. We attribute this phase to electron leakage to free semiquinone, which disproportionates into quinone and quinol (i.e.,  $2Q^- + 2H^+ \rightarrow Q + QH_2$ ) (55). Thus, to minimize any contribution of electron leakage to our measured values for  $\Phi_B$ , we performed the experiments with a minimum amount of added quinone required to occupy the  $Q_B$  site.

**Determination of the Quantum Efficiency  $\Phi_B$ .** The quantum efficiency  $\Phi_B$  of electron transfer to  $Q_B$  was determined in samples containing 2–3-fold UQ/RC and  $\sim 5 \mu\text{M}$  ferricyanide. Under these conditions essentially all observed kinetics was due to reduction of  $Q_B$ .  $\Phi_B$  was determined by two methods. In method 1,  $\Phi_B$  was obtained from the relative absorbance change in response to a single saturating laser flash (see top of Figure 2). However, for RCs with a low value of  $\Phi_B$ , the absorbance changes are small and consequently the uncertainty in  $\Phi_B$  relatively large. For example, in the single AW(M260) mutant RC,  $\Phi_B = 0.5\% \pm 0.3\%$ . In method 2,  $\Phi_B$  was obtained by fitting eq 4 to the rate of formation of charge separation following a train of saturating laser flashes. This gave a value of  $\Phi_B = 0.4\% \pm 0.1\%$  in the single mutant [AW(M260)] RC (Figure 2). The recombination rate constant  $k_{BD}$  was determined by fitting eq 5 to the absorption decay following the termination of the flash train. The fit of eq 4 to the data showed a small deviation ( $\sim 5\%$ ), which could be due to a small residual electron leakage from the excited RC to exogenous quinone. Analogous measurements made in the presence of substoichiometric quinone yielded similar values for  $\Phi_B$ . However, under these conditions the signal amplitude was smaller due to a lower  $Q_B$  occupancy.

The same two methods were used to determine  $\Phi_B$  in the other mutant RCs. A comparison of the experimental data using method 2 for the single AW(M260), double LH(M214)/AW(M260), quintuple, and native RCs is shown in Figure 3. The relative rates of signal generation and the steady-state values are determined almost entirely by the

Table 1: Quantum Efficiency  $\Phi$  and Recombination Rates  $k_{BD}$  in Native and Mutant RCs<sup>a</sup>

reaction center	$\Phi$ (%)	$k_{BD}$ (s <sup>-1</sup> )
native	100	0.74
AW(M260)	0.4	0.18
GD(M203)/AW(M260)	0.6	0.17
LH(M214)/AW(M260)	3.0	0.20
GD(M203)/LH(M214)/AW(M260)	3.0	0.16
FY(L181)/LH(M214)/AW(M260)	3.7	0.15
YF(M210)/LH(M214)/AW(M260)	4.1	0.17
FY(L181)/YF(M210)/LH(M214)/AW(M260)	5.0	0.14
FY(L181)/GD(M203)/YF(M210)/LH(M214)/AW(M260)	5.0	0.16

<sup>a</sup> The statistical uncertainty is  $\sim \pm 10\%$  of the reported value, except for the AW(M260) and GD(M203)/AW(M260) mutants for which the uncertainty is  $\pm 25\%$  of the reported value. Note that in the native RC  $\Phi$  measures the quantum efficiency along the A-branch,  $\Phi_A$ , and  $k_{BD}$  represents the *indirect* recombination through the higher energy  $Q_A^{\bullet-}$  state ( $D^+Q_AQ_B^{\bullet-} \leftrightarrow D^+Q_A^{\bullet-}Q_B \rightarrow DQ_AQ_B$ ). The value of  $\Phi_A$  was determined from a comparison of the amount of charge-separated state  $D^+Q_A^{\bullet-}$  generated following a single laser flash compared to the maximum absorbance change (see, e.g., Figure 3). In all of the mutant RCs, the A-branch is blocked. Thus,  $\Phi$  measures the quantum efficiency to  $Q_B$  along the B-branch,  $\Phi_B$ , and  $k_{BD}$  is the *direct* recombination back to the ground state ( $D^+Q_B^{\bullet-} \rightarrow DQ_B$ ). The values of  $\Phi_B$  were determined from the fit of eqs 4 and 5 to the measured generation and recovery of the charge-separated state  $D^+Q_B^{\bullet-}$  using a train of laser pulses as shown in Figure 2.

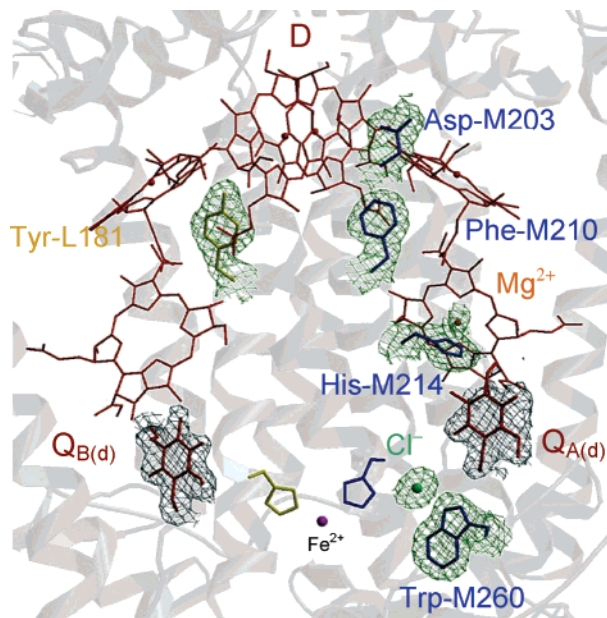


FIGURE 4: Part of the crystal structure of the quintuple mutant RC. The cofactors are shown in red imbedded within the backbone structure of the RC in gray. Shown are the electron densities (blue-green) and the side chains for the site-directed amino acid replacements Ala-M260 to Trp, Gly-M203 to Asp, Tyr-M210 to Phe, Leu-M214 to His (blue), and Phe-L181 to Tyr (yellow). As a consequence of the Ala-M260 to Trp replacement, a  $Cl^-$  anion (green) binds to the RC interacting with the nitrogen atoms of Trp-M260, His-M219, and Trp-M258 (not shown). An additional quinone  $Q_{A(d)}$  (red) was bound nearby, stacked between Trp-M268 and Phe-M258 (not shown), with the phenolic ring of Phe-M258 rotated to allow the quinone ring to intercalate between it and Trp-M268. The Leu-M214 to His replacement results in the incorporation of a  $Mg^{2+}$  atom (orange) into the bacteriopeophytin,  $H_A$ , transforming it to a bacteriochlorophyll,  $\beta_A$  (18). Note that  $Q_B$  binds in the distal position (labeled  $Q_{B(d)}$ ) as found by Ermler et al. (56) and Stowell et al. (15). (PDB accession code 1YF6.)

quantum efficiency  $\Phi_B$  (eq 4) since all mutants had similar values of  $k_{BD}$  (Table 1). Thus, one can see qualitatively an increase of  $\Phi_B$  from the single to the double, quintuple, and native RCs. The values of  $\Phi_B$  for the native and mutant RCs

are summarized in Table 1. For all of the mutant samples, both methods agreed within experimental uncertainty with each other, with method 2 providing more precise values. The largest values of  $\Phi_B$  ( $\sim 5\%$ ) were obtained in the FY-(L181)/YF(M210)/LH(M214)/AW(M260) and FY(L181)/GD(M203)/YF(M210)/LH(M214)/AW(M260) (quintuple) mutant RCs.

*Structure of the Quintuple Mutant RC.* X-ray data were collected on trigonal crystals (space group  $P3_121$ ) to a resolution of 2.25 Å (85% complete). The ratio of the average of the diffraction intensities to the average background intensity was 6.6. The structure was refined to an  $R$ -factor of 19.6 ( $R_{free} = 21.6$ ) with no residues in disallowed regions. The overall backbone structure of the mutant RC is essentially the same as that of the native RC (15). All changes were localized near the side chain replacements with three major exceptions: (i) the displacement of  $Q_A$  and the binding of a  $Cl^-$  anion due to the Ala-M260 replacement with Trp, (ii) the binding of a quinone to a new location due to the rearrangement of the M258 and M268 side chains, and (iii) the creation of a bacteriochlorophyll  $\beta_A$  at the  $H_A$  site due to the replacement of Leu by His at M214.

The displacement of  $Q_A$  from its binding pocket was shown in the structure by the lack of electron density associated with a quinone molecule at this location (39). This was attributed to the replacement of Ala with Trp at M260 in which the much larger Trp side chain occupies a large part of the  $Q_A$  binding site. An additional consequence of the M260 replacement is the presence of a  $Cl^-$  anion bound near His-M219 and Trp-M260 (Figure 4). These same changes were found in the single AW(M260) mutant structure (39).

A new result observed in the structure was the binding of a quinone ring at a new location near Phe-M258 and Trp-M268. The side chains of Phe-M258 and Trp-M268 were rearranged to allow a quinone ring to intercalate between them. The observed density was assigned to a quinone ring based on its size, shape, and its presence following the soaking of the crystals in artificial mother liquor containing excess quinone. Although the density of the headgroup was well resolved, the positions of the carbonyl oxygens were not. This indicates some rotational freedom suggesting weak (if any) hydrogen bonding. Among the side chain rearrangements was the rotation of the phenolic ring of Phe-M258. In the native structure, Phe-M258 forms part of the binding region for the isoprenoid tail of  $Q_A$ . In the absence of the isoprenoid tail of  $Q_A$ , the side chain of Phe-M258 is free to rotate and reorient to provide part of a hydrophobic pocket that binds the headgroup of a quinone molecule. This differs from the McAuley work (39) in which these changes were not reported. We attribute this difference to the fact that in our work excess quinone was added to crystals of the quintuple mutant prior to data collection.

The position of this quinone is approximately symmetrically located with respect to the "distal"  $Q_B$  position as determined by Ermler et al. (56) and Stowell et al. (15) (Figure 4). It is located within 4.5 Å of the edge of  $\beta_A$ . This places the quinone closer to  $\beta_A$  by  $\sim 2$  Å than the position of  $Q_A$  to  $H_A$  in the native structure (15, 45, 46).

The change of  $H_A$  to a bacteriochlorophyll  $\beta_A$  due to the replacement of Leu by His was shown by the presence of electron density in the middle of the porphyrin ring at the

$H_A$  site assigned to a  $Mg^{2+}$  ion (Figure 4). The presence of the bacteriochlorophyll was also shown by the increase in the optical spectrum at 800 nm and a decrease at 760 nm (18). A water molecule near  $B_A$  due to the replacement of Gly by Asp at M203 was displaced as has been previously reported (57).

Since these studies focus on the B-side electron transfer, it is worth noting that (i) there are no changes observed in the cofactor structures along the B-branch and (ii)  $Q_B$  is located predominantly at the distal position as reported in the native structure by Emler et al. (56) and Stowell et al. (15).

## DISCUSSION

In this work we report on the construction and characterization of mutant RCs designed to form  $Q_B^{-\bullet}$  via electron transfer along the B-branch of the RC. The new constructs reported here combine several mutations previously shown to increase B-branch electron transfer, mostly in *Rb. capsulatus* (16–32), with a mutation to eliminate the native electron transfer pathway by removing  $Q_A$  (34, 38, 39). Electron transfer through the B-branch occurs via  $H_B^{-\bullet}$ , which has a much lower redox potential than the native  $Q_A^{-\bullet}$ . This increases the driving force and rate of electron transfer to  $Q_B$  (16), thereby enabling intermediate states to be trapped which are energetically or kinetically inaccessible in the native system. We shall discuss the evidence for the generation of reduced  $Q_B$  via B-branch electron transfer, the determination of the quantum efficiency along the B-branch to  $Q_B$ ,  $\Phi_B$ , the rate of electron transfer from  $H_B^{-\bullet}$  to  $Q_B$ , the determination of the A-branch to B-branch electron transfer ratio, and the binding and function of quinones in the mutant RC and propose future work to increase  $\Phi_B$  and to investigate high-energy intermediate states.

**Evidence for Generating the  $D^{+\bullet}Q_B^{-\bullet}$  State.** Evidence that the charge-separated state generated in the mutant RCs upon excitation with light is the  $D^{+\bullet}Q_B^{-\bullet}$  state is provided by (1) the sensitivity of its formation to known  $Q_B$  inhibitors such as terbutryne and stigmatellin and (2) the recombination rate of  $\sim 0.17\text{ s}^{-1}$ , which is the same as that determined for direct recombination from  $Q_B^{-\bullet}$  to  $D^{+\bullet}$  (52–54). This is in agreement with reports by Laible et al. (33) and Wakeham et al. (34, 35) and is supported by FTIR studies on B-branch mutant RCs by Breton et al. (36). Since  $Q_A$  is lacking in the mutant RCs (Figure 4), formation of  $Q_B^{-\bullet}$  cannot occur via  $Q_A^{-\bullet}$  (A-branch). Since similar values were measured in the absence of excess quinone, formation of  $Q_B^{-\bullet}$  cannot be due to electron transfer through  $Q_{A(d)}$ . Thus,  $Q_B^{-\bullet}$  is formed via B-branch electron transfer from  $H_B^{-\bullet}$  (Figure 1) as was shown previously (16, 33–36, 40, 41).

**Quantum Efficiency along the B-Branch,  $\Phi_B$ .** The quantum efficiency of electron transfer to  $Q_B$  along the B-branch,  $\Phi_B$ , was determined using two methods based on absorption changes in response to a single or a train of saturating laser flashes (Figure 2) (see Materials and Methods). The results are summarized in Table 1. The smallest value of  $\Phi_B = 0.4\% \pm 0.1\%$  was observed in the single AW(M260) mutant RC, in which  $Q_A$  has been displaced by Trp-M260. Upon addition of other mutations,  $\Phi_B$  increased from 0.4% to 5%. The largest values of  $\Phi_B$  were observed in mutant RCs that had the LH(M214) mutation. The effect of this mutation is the

assembly of a bacteriochlorophyll,  $\beta_A$ , in the  $H_A$  site (Figure 4). In solution, a bacteriochlorophyll is more difficult to reduce by  $\sim 200\text{--}300\text{ meV}$  than bacteriopheophytin (58, 59). Analogously in the RC,  $\beta_A$  is more difficult to reduce than  $H_A$ . This decreases the effectiveness of the A-branch electron transfer relative to the B-branch.

How do these results compare with previously measured values? We can compare our results with two reports in *Rb. sphaeroides*. In one the GD(M203)/LH(M214)/AW(M260) RC yielded a value of  $\sim 3\%$  for B-branch electron transfer to  $H_B$  (32), which is in good agreement with our value of 3% for B-branch electron transfer to  $Q_B$  (Table 1). In contrast, in another report a value of  $\sim 7\%$  for B-branch electron transfer to  $H_B$  was measured in the GD(M203)/AW(M260) (29), which is considerably larger than our value of 0.6% for electron transfer to  $Q_B$ . One likely explanation is that the rate of electron transfer from  $H_B^{-\bullet}$  to  $Q_B$  is particularly slow in this mutant RC.

The largest value for  $\Phi_B$  that we observed was  $\sim 5\%$ , which is considerably lower than the 25% to  $H_B$  observed in B-branch mutants of *Rb. capsulatus* (16). This result is consistent with previous observations of lower B-branch quantum efficiency in *Rb. sphaeroides* mutants than in similar mutants of *Rb. capsulatus* (29). We explain this difference by invoking the previous supposition that the relative energy levels of the cofactors along each branch differ in the two bacterial species (29), resulting in the different effects of the mutations.

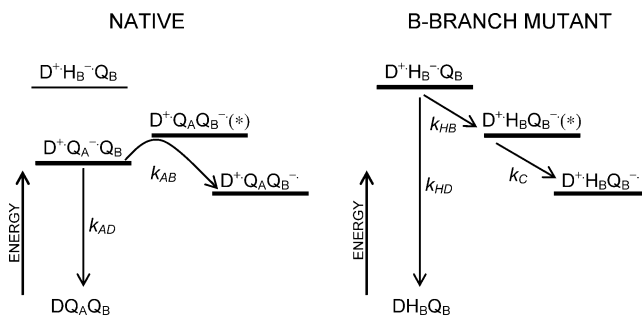


FIGURE 5: Schematic representation of the energy levels for the ground and charge-separated states formed by light-induced electron transfer in the native RC (left) and in the mutants (right). Excitation of the primary donor, D, by light (not shown) leads to electron transfer resulting in the charge-separated state  $D^{+\bullet}Q_A^{-\bullet}Q_B$  (native RC) or  $D^{+\bullet}H_B^{-\bullet}Q_B$  (mutant RC). The states involved in subsequent electron transfer are indicated by heavy lines.  $k_{AB}$  and  $k_{HB}$  are the forward electron transfer rate constants, and  $k_{AD}$  and  $k_{HD}$  are the charge recombination rate constants for the native and mutant RCs, respectively;  $k_C$  is the rate at which the intermediate  $D^{+\bullet}H_BQ_B^{-\bullet}$  state is converted to the final  $D^{+\bullet}H_BQ_B^{-\bullet}$  state. In the native RC, the quantum efficiency  $\Phi_A$  of electron transfer to form the  $D^{+\bullet}Q_A^{-\bullet}Q_B$  state is nearly 100%. Thermally activated electron transfer through the intermediate  $D^{+\bullet}Q_AQ_B^{-\bullet}$  state results in the formation of the  $D^{+\bullet}Q_AQ_B^{-\bullet}$  state. In the mutant RC, the quantum efficiency  $\Phi_B$  of electron transfer to  $Q_B$  is determined by the efficiency of forming  $D^{+\bullet}H_B^-Q_B$  and the efficiency of subsequent electron transfer to form  $D^{+\bullet}H_BQ_B^{-\bullet}$ , which is determined by the branching ratio  $k_{HB}/(k_{HB} + k_{HD})$ . A value of  $\Phi_B$  of  $\sim 5\%$  was achieved in the quintuple B-branch mutant RC. Since  $D^{+\bullet}H_B^-Q_B$  has a higher free energy than that of  $D^{+\bullet}Q_A^-Q_B$ , the formation of the intermediate state  $D^{+\bullet}H_BQ_B^{-\bullet}$  is favorable. In contrast, in the native RC the intermediate state  $D^{+\bullet}Q_AQ_B^{-\bullet}$  is thermally activated and therefore not significantly populated.

**Rate of Electron Transfer from  $H_B^{-\bullet}$  to  $Q_B$ .** The studies reported in this work address the net transfer efficiency to

$Q_B$  via B-branch electron transfer, which could differ from the more commonly reported quantum efficiency for electron transfer to  $H_B$ . A difference would be observed if the electron transfer efficiency from  $H_B^{-\bullet}$  to  $Q_B$  were less than 100%. This would occur when the recombination to the ground state,  $k_{HD}$ , competes with the forward electron transfer,  $k_{HB}$  (see Figure 5), resulting in a transfer efficiency from  $H_B^{-\bullet}$  to  $Q_B$  of  $k_{HB}/(k_{HB} + k_{HD})$  (16).

The values of  $k_{HB}$  and  $k_{HD}$  have not been determined in *Rb. sphaeroides*. However, since our experimental results are within a factor of 2 the same as those reported in mutant RCs of *Rb. capsulatus* by Kirmaier et al. (16), we shall assume that their estimate for  $k_{HB} = (1-5) \times 10^8 \text{ s}^{-1}$  in *Rb. capsulatus* is the same within a factor of 2 for *Rb. sphaeroides* (16). This rate constant is 10–50-fold smaller than the corresponding rate constant,  $k_{HA}$ , for electron transfer from  $H_A^{-\bullet}$  to  $Q_A$  along the A-branch in the native RC (17). This can be explained by a change in the reorganization energy ( $\lambda$ ) for electron transfer due to the more polar nature of the  $Q_B$  site. It had been shown that the  $\sim 70$ -fold slower recombination rate from  $Q_B^{-\bullet}$  to  $D^{+\bullet}$  compared to  $Q_A^{-\bullet}$  to  $D^{+\bullet}$  is due to a difference in  $\lambda$  of  $\sim 500 \text{ meV}$  (53). Analogously, the difference in  $\lambda$  would also decrease electron transfer to  $Q_B$  compared to  $Q_A \sim 70$ -fold if other factors such as the electron transfer tunneling pathway and free energy for electron transfer are the same. Furthermore, this explanation suggests that the movement of  $Q_B$  from the distal location (Figure 4) to the proximal location at which  $Q_B^{-\bullet}$  prefers to bind (15, 46) is not the rate-controlling step for electron transfer from  $H_B^{-\bullet}$  to  $Q_B$ .

**The A-Branch to B-Branch Electron Transfer Ratio.** From the determination of the value of  $\Phi_B$  in the AW(M260) single mutant, we can calculate the branching ratio of A-branch to B-branch electron transfer in the mutant RC. We assume that the value of  $\Phi_B$  (0.4%) determined in the AW(M260) mutant is the same as in the native RC where it is masked by the predominant electron transfer through the A-branch ( $\Phi_A \cong 100\%$ ). Thus, we obtain a branching ratio of  $\Phi_A/\Phi_B$  of  $250 \pm 100$ , which is consistent with the limits previously established (17, 20, 60–63). Further validation of this result will require the measurement of  $k_{HD}$  (Figure 5) in the mutant RC.

**The Binding and Function of Quinones.** In the quintuple mutant RC, there are two quinone molecules observed in the structure. One is the presence of  $Q_B$  located predominantly at the distal position. Since this is the same as reported for the native RC by Ermler et al. (56) and Stowell et al. (15), the mutation at M260, which results in the removal of  $Q_A$  and the binding of  $Cl^-$ , does not induce a change in the preferred binding position of the neutral  $Q_B$ . This finding is in contrast to the results of McAuley et al. (39), who reported the position of  $Q_B$  at the proximal site. Although we have no definitive explanation for the reported discrepancies of the  $Q_B$  position (46, 64), we have found that  $Q_B^{-\bullet}$  can be inadvertently trapped in the proximal position (e.g., with background light) in the AW(M260) mutant RC (data not shown), which may account for the increased electron density

at the proximal location reported by McAuley et al. (39).<sup>2</sup>

Another quinone molecule  $Q_{A(d)}$  was located near the native  $Q_A$  region at a position roughly symmetrically related to the distal  $Q_B$  position (Figure 4). The quinone headgroup was stacked between Trp-M268 and Phe-M258, which had rearranged to permit the intercalation of the quinone headgroup between the aromatic side chains. However, the charge recombination measurements (see, e.g., eq 6 fit in Figure 2) show only a single decay rate due to recombination of  $D^{+\bullet}Q_B^{-\bullet}$ , indicating that  $Q_{A(d)}$  is nonfunctional; i.e., it cannot be stably reduced. This is not the result of a larger tunneling distance for electron transfer since the distance from  $Q_{A(d)}$  to  $\beta_A$  is even shorter than  $Q_A$  to  $H_A$  in the native RC (15, 56). We attribute the lack of reduction of  $Q_{A(d)}$  to weak (or the absence of) hydrogen bonds, which in the native RC stabilizes  $Q_A^{-\bullet}$  (65–69).

**Future Work: Increase  $\Phi_B$  and Trap Intermediate States.** We have obtained a maximum quantum yield for B-branch electron transfer to  $Q_B$  of  $\Phi_B = 5\%$ . Our plan is to attempt to increase this value. One approach is to introduce additional mutations designed to increase  $\Phi_B$  such as HL(M182), which has been shown to increase electron transfer to  $H_B$  in *Rb. sphaeroides* (23, 31). Another approach is to decrease the recombination rate  $k_{HD}$  to a value significantly smaller than  $k_{HB}$  by replacing residues located along the “tunneling” pathway between  $H_B$  and D, such as replacing Phe-L181 with the smaller Ala. This will increase  $\Phi_B$  by increasing the transfer efficiency from  $H_B^{-\bullet}$  to  $Q_B$  given by  $k_{HB}/(k_{HB} + k_{HD})$ .

Having established a system in which  $Q_B^{-\bullet}$  can be formed via B-branch electron transfer, we can now trap intermediate states in the  $Q_B$  reduction process. This is made possible because  $D^{+\bullet}H_B^{-\bullet}Q_B$ , which is formed in the B-branch mutant RC, has a higher free energy than  $D^{+\bullet}Q_A^{-\bullet}Q_B$ , so the formation of intermediate state  $D^{+\bullet}H_BQ_B^{-\bullet(*)}$  with an energy between  $D^{+\bullet}H_B^{-\bullet}Q_B$  and  $D^{+\bullet}Q_A^{-\bullet}Q_B$  is favorable (see Figure 5). If  $k_C$  is thermally activated,  $D^{+\bullet}H_BQ_B^{-\bullet(*)}$  can be accumulated and trapped at low temperature. We have been able to trap  $D^{+\bullet}H_BQ_B^{-\bullet(*)}$  by freezing the B-branch mutant RC prior to excitation by light. The trapped  $D^{+\bullet}H_BQ_B^{-\bullet(*)}$  state had a recombination rate that was  $>10^6$ -fold larger than that of  $D^{+\bullet}H_BQ_B^{-\bullet}$ , which was formed by freezing under illumination (41). This shows that there are two (or more) distinct reducible  $Q_B$  states (Figure 5) that can be accessed in B-branch mutant RCs (41). We plan to use EPR spectroscopy to further probe the electronic structure of  $Q_B^{-\bullet}$  and  $Q_B^{-\bullet(*)}$  (see Figure 5) (69).

## ACKNOWLEDGMENT

DNA sequencing was performed by the DNA Sequencing Shared Resource, UCSD Cancer Center, which is funded in part by NCI Cancer Center Support Grant 2 P30 CA23100-18.

## SUPPORTING INFORMATION AVAILABLE

A table of the X-ray data collection and refinement statistics for the structure determination of the quintuple

<sup>2</sup> In the course of this work, we had inadvertently trapped up to 45%  $Q_B^{-\bullet}$  in B-branch mutant RCs lacking  $Q_A$ . This was presumably due to ambient room light illumination. The trapped  $Q_B^{-\bullet}$  was oxidized to  $Q_B$  by the addition of ferricyanide (51) to obtain a well-defined starting state.

mutant RC. This material is available free of charge via the Internet at <http://pubs.acs.org>.

## REFERENCES

- Okamura, M. Y., and Feher, G. (1992) Proton transfer in reaction centers from photosynthetic bacteria, *Annu. Rev. Biochem.* **61**, 861–896.
- Blankenship, R. E., Madigan, M. T., and Bauer, C. E. (1995) *Anoxygenic photosynthetic bacteria*, Vol. 2, Kluwer Academic Publishers, Dordrecht, The Netherlands.
- Vermeglio, A. (1977) Secondary electron transfer in reaction centers of *Rhodospseudomonas sphaeroides*. Out-of-phase periodicity of two for the formation of ubisemiquinone and fully reduced ubiquinone, *Biochim. Biophys. Acta* **459**, 516–524.
- Kleinfeld, D., Okamura, M. Y., and Feher, G. (1984) Electron transfer in reaction centers of *Rhodospseudomonas sphaeroides*. I. Determination of the charge recombination pathway of  $D^+Q_AQ_B^-$  and free energy and kinetic relations between  $Q_AQ_B^-$  and  $Q_AQ_B^-$ , *Biochim. Biophys. Acta* **766**, 126–140.
- Tiede, D. M., Vazquez, J., Cordova, J., and Marone, P. A. (1996) Time-resolved electrochromism associated with the formation of quinone anions in the *Rhodobacter sphaeroides* R26 reaction center, *Biochemistry* **35**, 10763–10775.
- Graige, M. S., Feher, G., and Okamura, M. Y. (1998) Conformation gating of the electron transfer reaction  $Q_A^-Q_B^- \rightarrow Q_AQ_B^-$ , in bacterial reaction centers of *Rb. sphaeroides* determined by a driving force assay, *Proc. Natl. Acad. Sci. U.S.A.* **95**, 11679–11684.
- Wraight, C. A. (1979) Electron acceptors of bacterial photosynthetic reaction centers: II.  $H^+$  binding coupled to secondary electron transfer in the quinone acceptor complex, *Biochim. Biophys. Acta* **548**, 309–327.
- Kleinfeld, D., Okamura, M. Y., and Feher, G. (1985) Electron transfer in reaction centers from *Rhodospseudomonas sphaeroides*. II. Free energy and kinetic relations between the acceptor states  $Q_A^-Q_B^-$  and  $Q_AQ_B^-$ , *Biochim. Biophys. Acta* **809**, 291–310.
- Paddock, M. L., Feher, G., and Okamura, M. Y. (2003) Proton-transfer pathways and mechanism in bacterial reaction centers, *FEBS Lett.* **555**, 45–50.
- Feher, G., Allen, J. P., Okamura, M. Y., and Rees, D. C. (1989) Structure and function of photosynthetic reaction centers, *Nature* **339**, 111–116.
- Gunner, M. R. (1991) The reaction center protein from purple bacteria structure and function, *Curr. Top. Bioenerg.* **16**, 319–367.
- Hoff, A. J., and Deisenhofer, J. (1997) Photophysics of photosynthesis: structure and spectroscopy of reaction centers of purple bacteria, *Phys. Rep.* **287**, 2–247.
- Graige, M. S., Paddock, M. L., Bruce, J. M., Feher, G., and Okamura, M. Y. (1996) Mechanism of proton-coupled electron transfer for quinone ( $Q_B$ ) reduction in reaction centers of *Rb. sphaeroides*, *J. Am. Chem. Soc.* **118**, 9005–9016.
- Xu, Q., and Gunner, M. R. (2001) Trapping conformational intermediate states in the reaction center protein from photosynthetic bacteria, *Biochemistry* **40**, 3232–3241.
- Stowell, M. H., McPhillips, T. M., Rees, D. C., Soltis, S. M., Abresch, E., and Feher, G. (1997) Light-induced structural changes in photosynthetic reaction center: implications for mechanism of electron–proton transfer, *Science* **276**, 812–816.
- Kirmaier, C., Laible, P. D., Hanson, D. K., and Holten, D. (2003) B-side charge separation in bacterial photosynthetic reaction centers: nanosecond time scale electron transfer from  $H_B^-$  to  $Q_B$ , *Biochemistry* **42**, 2016–2024.
- Kirmaier, C., Holten, D., and Parson, W. W. (1985) Temperature and detection-wavelength dependence of the picosecond electron transfer kinetics measured in *Rhodospseudomonas sphaeroides* reaction centers of new spectral and kinetic components in the primary charge separation process, *Biochim. Biophys. Acta* **810**, 33–48.
- Kirmaier, C., Gaul, D., DeBey, R., Holten, D., and Schenck, C. C. (1991) Charge separation in a reaction center incorporating bacteriochlorophyll for photoactive bacteriopeophytin, *Science* **251**, 922–927.
- Kirmaier, C., Laporte, L., Schenck, C. C., and Holten, D. (1995) The nature and dynamics of the charge-separated intermediate in reaction centers in which bacteriochlorophyll replaces the photoactive bacteriopeophytin. 2. The rates and yields of charge separation and recombination, *J. Phys. Chem.* **99**, 8910–8917.
- Heller, B. A., Holten, D., and Kirmaier, C. (1995) Control of electron transfer between the L- and M-sides of photosynthetic reaction centers, *Science* **269**, 940–945.
- Heller, B. A., Holten, D., and Kirmaier, C. (1996) Effects of Asp residues near the L-side pigments in bacterial reaction centers, *Biochemistry* **35**, 15418–15427.
- Kirmaier, C., Weems, D., and Holten, D. (1999) M-side electron transfer in reaction center mutants with a lysine near the nonphotoactive bacteriochlorophyll, *Biochemistry* **38**, 11516–11530.
- Katilius, E., Turanchik, T., Lin, S., Taguchi, A. K. W., and Woodbury, N. W. (1999) B-Side electron transfer in a *Rhodobacter sphaeroides* reaction center mutant in which the B-side monomer bacteriochlorophyll is replaced with bacteriopeophytin, *J. Phys. Chem. B* **103**, 7386–7389.
- Lin, S., Jackson, J. A., Taguchi, A. K. W., and Woodbury, N. W. (1999) B-Side electron transfer promoted by absorbance of multiple photons in *Rhodobacter sphaeroides* R-26 reaction centers, *J. Phys. Chem. B* **103**, 4757–4763.
- Lin, S., Katilius, E., Haffa, A. L., Taguchi, A. K., and Woodbury, N. W. (2001) Blue light drives B-side electron transfer in bacterial photosynthetic reaction centers, *Biochemistry* **40**, 13767–13773.
- Roberts, J. A., Holten, D., and Kirmaier, C. (2001) Primary events in photosynthetic reaction centers with multiple mutations near the photoactive electron carriers, *J. Phys. Chem. B* **105**, 5575–5584.
- Kirmaier, C., He, C., and Holten, D. (2001) Manipulating the direction of electron transfer in the bacterial reaction center by swapping Phe for Tyr near  $BChl_M$  (L181) and Tyr for Phe near  $BChl_L$  (M208), *Biochemistry* **40**, 12132–12139.
- Katilius, E., Katiliene, Z., Lin, S., Taguchi, A. K. W., and Woodbury, N. W. (2002) B-Side electron transfer in a *Rhodobacter sphaeroides* reaction center mutant in which the B side monomer bacteriochlorophyll is replaced with bacteriopeophytin: Low-temperature study and energetics of charge-separated states, *J. Phys. Chem. B* **106**, 1471–1475.
- Kirmaier, C., Laible, P. D., Czarnecki, K., Hata, A. N., Hanson, D. K., Bocian, D. F., and Holten, D. (2002) Comparison of M-side electron transfer in *Rb. sphaeroides* and *Rb. capsulatus* reaction centers, *J. Phys. Chem. B* **106**, 1799–1808.
- Kirmaier, C., Cua, A., He, C., Holten, D., and Bocian, D. F. (2002) Probing M-branch electron transfer and cofactor environment in the bacterial photosynthetic reaction center by addition of a hydrogen bond to the M-side bacteriopeophytin, *J. Phys. Chem. B* **106**, 495–503.
- de Boer, A. L., Neerken, S., de Wijn, R., Permentier, H. P., Gast, P., Vijgenboom, E., and Hoff, A. J. (2002) High yield of B-branch electron transfer in a quadruple reaction center mutant of the photosynthetic bacterium *Rhodobacter sphaeroides*, *Biochemistry* **41**, 3081–3088.
- de Boer, A. L., Neerken, S., de Wijn, R., Permentier, H. P., Gast, P., Vijgenboom, E., and Hoff, A. J. (2002) B-branch electron transfer in reaction centers of *Rhodobacter sphaeroides* assessed with site-directed mutagenesis, *Photosynth. Res.* **71**, 221–239.
- Laible, P. D., Kirmaier, C., Udawatte, C. S., Hofman, S. J., Holten, D., and Hanson, D. K. (2003) Quinone reduction via secondary B-branch electron transfer in mutant bacterial reaction centers, *Biochemistry* **42**, 1718–1730.
- Wakeham, M. C., Goodwin, M. G., McKibbin, C., and Jones, M. R. (2003) Photoaccumulation of the  $P^+Q_B^-$  radical pair state in purple bacterial reaction centres that lack the  $Q_A$  ubiquinone, *FEBS Lett.* **540**, 234–240.
- Wakeham, M. C., Breton, J., Nabedryk, E., and Jones, M. R. (2004) Formation of a semiquinone at the  $Q_B$  site by A- or B-branch electron transfer in the reaction center from *Rhodobacter sphaeroides*, *Biochemistry* **43**, 4755–4763.
- Breton, J., Wakeham, M. C., Fyfe, P. K., Jones, M. R., and Nabedryk, E. (2004) Characterization of the bonding interactions of  $Q_B$  upon photoreduction via A-branch or B-branch electron transfer in mutant reaction centers from *Rhodobacter sphaeroides*, *Biochim. Biophys. Acta* **1656**, 127–138.
- Williams, J. C., Alden, R. G., Murchison, H. A., Peloquin, J. M., Woodbury, N. W., and Allen, J. P. (1992) Effects of mutations near the bacteriochlorophylls in reaction centers from *Rhodobacter sphaeroides*, *Biochemistry* **31**, 11029–11037.

38. Ridge, J. P., van Brederode, M. E., Goodwin, M. G., van Grondelle, R., and Jones, M. R. (1999) Mutations that modify or exclude binding of the Q<sub>A</sub> ubiquinone and carotenoid in the reaction center from *Rhodobacter sphaeroides*, *Photosynth. Res.* 59, 9–26.
39. McAuley, K. E., Fyfe, P. K., Ridge, J. P., Cogdell, R. J., Isaacs, N. W., and Jones, M. R. (2000) Ubiquinone binding, ubiquinone exclusion, and detailed cofactor conformation in a mutant bacterial reaction center, *Biochemistry* 39, 15032–15043.
40. Paddock, M. L., Isaacson, R., Chang, C., Feher, G., and Okamura, M. Y. (2004) Conformations of Q<sub>B</sub><sup>-</sup> trapped by B side electron transfer in reaction centers from *Rhodobacter sphaeroides*, *Biophys. J.* 86, 11a.
41. Paddock, M. L., Flores, M., Isaacson, R. I., Chang, C., Abresch, E. C., Selvaduray, P., Feher, G., and Okamura, M. Y. (2005) Q<sub>B</sub><sup>-</sup> formation by B-branch electron transfer in reaction centers from *Rhodobacter sphaeroides*, in *Photosynthesis: Fundamental Aspects to Global Perspectives* (van der Est, A., and Bruce, D., Eds.) Allen Press, Lawrence, KS (in press).
42. Paddock, M. L.; Adéloth, P., Chang, C., Abresch, E. C., Feher, G., and Okamura, M. Y. (2001) Identification of the proton pathway in bacterial reaction centers: cooperation between Asp-M17 and Asp-L210 facilitates proton transfer to the secondary quinone (Q<sub>B</sub>), *Biochemistry* 40, 6893–6902.
43. Paddock, M. L., Rongey, S. H., Abresch, E. C., Feher, G., and Okamura, M. Y. (1988) Reaction centers from three herbicide resistant mutants of *Rhodobacter sphaeroides* 2.4.1: Sequence analysis and preliminary characterization, *Photosynth. Res.* 17, 75–96.
44. McElroy, J. D., Mauzerall, D. C., and Feher, G. (1974) Characterization of primary reactants in bacterial photosynthesis II. Kinetic studies of the light-induced signal ( $g = 2.0026$ ) and the optical absorbance changes at cryogenic temperatures, *Biochim. Biophys. Acta* 333, 261–278.
45. Buchanan, S. K., Fritzsche, G., Ermler, U., and Michel, H. (1993) New crystal form of the photosynthetic reaction centre from *Rhodobacter sphaeroides* of improved diffraction quality, *J. Mol. Biol.* 230, 1311–1314.
46. Fritzsche, G., Koepke, J., Diem, R., Kuglstatter, A., and Baciou, L. (2002) Charge separation induces conformational changes in the photosynthetic reaction centre of purple bacteria, *Acta Crystallogr. D* 58, 1660–1663.
47. Xu, Q., Axelrod, H. L., Abresch, E. C., Paddock, M. L., Okamura, M. Y., and Feher, G. (2004) X-ray structure determination of three mutants of the bacterial photosynthetic reaction centers from *Rb. sphaeroides*: Altered proton-transfer pathways, *Structure* 12, 703–715.
48. Leslie, A. G. W. (1992) *Joint CCP4 and ESF-EACMB Newsletter on Protein Crystallography*, Daresbury Laboratory, Warrington, U.K.
49. Brunger, A. T., Adams, P. D., Clore, G. M., DeLano, W. L., Gros, P., Grosse-Kunstleve, R. W., Jiang, J.-S., Kuszewski, J., Nilges, N., Pannu, N. S., Read, R. J., Rice, L. M., Simonson, T., and Warren, G. L. (1998) Crystallography and NMR system: A new software suite for macromolecular structure determination, *Acta Crystallogr. D* 54, 905–921.
50. McRee, D. E. (1999) XtalView/Xfit—A versatile program for manipulating atomic coordinates and electron density, *J. Struct. Biol.* 125, 156–165.
51. Wakeham, M. C., Frolov, D., Fyfe, P. K., van Grondelle, R., and Jones, M. R. (2003) Acquisition of photosynthetic capacity by a reaction centre that lacks the Q<sub>A</sub> ubiquinone; possible insights into the evolution of reaction centres?, *Biochim. Biophys. Acta* 1607, 53–63.
52. Labahn, A., Paddock, M. L., McPherson, P. H., Okamura, M. Y., and Feher, G. (1994) Direct charge recombination from D<sup>+</sup>Q<sub>A</sub>Q<sub>B</sub><sup>-</sup> to DQ<sub>A</sub>Q<sub>B</sub> in bacterial reaction centers from *Rhodobacter sphaeroides*, *J. Phys. Chem.* 98, 3417–3423.
53. Labahn, A., Bruce, J. M., Okamura, M. Y., and Feher, G. (1995) Direct charge recombination from D<sup>+</sup>Q<sub>A</sub>Q<sub>B</sub><sup>-</sup> to DQ<sub>A</sub>Q<sub>B</sub> in bacterial reaction centers from *Rhodobacter sphaeroides* containing low potential quinone in the Q<sub>A</sub> site, *Chem. Phys.* 197, 355–366.
54. Allen, J. P., Williams, J. C., Graige, M. S., Paddock, M. L., Labahn, A., Feher, G., and Okamura, M. Y. (1998) Free energy dependence of the direct charge recombination from the primary and secondary quinones in reaction centers from *Rhodobacter sphaeroides*, *Photosynth. Res.* 55, 227–233.
55. Roginsky, V. A., Pisarenko, L. M., Bors, W., and Michel, C. (1999) The kinetics and thermodynamics of quinone-semiquinone-hydroquinone systems under physiological conditions, *J. Chem. Soc., Perkin Trans. 2*, 871–876.
56. Ermler, U., Fritzsche, G., Buchanan, S. K., and Michel, H. (1994) Structure of the photosynthetic reaction centre from *Rhodobacter sphaeroides* at 2.65 Å resolution: cofactors and protein-cofactor interactions, *Structure* 2, 925–936.
57. Fyfe, P. K., Ridge, J. P., McAuley, K. E., Cogdell, R. J., Isaacs, N. W., and Jones, M. R. (2000) Structural consequences of the replacement of glycine M203 with aspartic acid in the reaction center from *Rhodobacter sphaeroides*, *Biochemistry* 39, 5953–5960.
58. Fajer, J., Brune, D. C., Davis, M. S., Forman, A., and Spaulding, L. D. (1975) Primary charge separation in bacterial photosynthesis: oxidized chlorophylls and reduced pheophytin, *Proc. Natl. Acad. Sci. U.S.A.* 72, 4956–4960.
59. Cotton, T. M., and Van Duyne, R. P. (1979) An electrochemical investigation of the redox properties of bacteriochlorophyll and bacteriochlorophytin in aprotic solvents, *J. Am. Chem. Soc.* 101, 7605–7612.
60. Holten, D., Windsor, M. W., Parson, W. W., and Thornber, J. P. (1978) Primary photochemical processes in isolated reaction centers of *Rhodospseudomonas viridis*, *Biochim. Biophys. Acta* 501, 112–126.
61. Bixon, M., Jortner, J., Michel-Beyerle, M.-E., and Ogrodnik, A. (1989) A Superexchange mechanism for the primary charge separation in photosynthetic reaction centers, *Biochim. Biophys. Acta* 977, 273–286.
62. Aumeier, W., Eberl, U., Ogrodnik, A., Volk, M., Scheidel, G., Feick, R., Plato, M., and Michel-Beyerle, M.-E. (1990) in *Current Research in Photosynthesis* (Baltscheffsky, M., Ed.) Vol. 1, pp 133–136, Kluwer Academic Publishers, Dordrecht, The Netherlands.
63. Woodbury, N. W., and Allen, J. P. (1995) in *Anoxygenic photosynthetic bacteria* (Blankenship, R. E., Madigan, M. T., and Bauer, C. E., Eds.) pp 527–557, Kluwer Academic Publishers, Dordrecht, The Netherlands.
64. Kuglstatter, A., Ermler, U., Michel, H., Baciou, L., and Fritzsche, G. (2001) X-ray structure analyses of photosynthetic reaction center variants from *Rhodobacter sphaeroides*: structural changes induced by point mutations at position L209 modulate electron and proton transfer, *Biochemistry* 40, 4253–4260.
65. Swallow, A. J. (1982) Physical Chemistry of Semiquinones, in *Function of Quinones in Energy Conserving Systems* (Trumpower, B. L., Ed.) pp 59–72, Academic Press, New York.
66. Prince, R. C., Gunner, M. R., and Dutton, P. L. (1982) Quinones of Value to Electron-Transfer Studies: Oxidation–Reduction Potentials of the First Reduction Step in an Aprotic Solvent, in *Function of Quinones in Energy Conserving Systems* (Trumpower, B. L., Ed.) pp 29–58, Academic Press, New York.
67. Alexov, E. G., and Gunner, M. R. (1997) Incorporating protein conformational flexibility into the calculation of pH-dependent protein properties, *Biophys. J.* 72, 2075–2093.
68. Grafton, A. K., and Wheeler, R. A. (1999) Amino acid protonation states determine binding sites of the secondary ubiquinone and its anion in the *Rhodobacter sphaeroides* photosynthetic reaction center, *J. Phys. Chem. B* 103, 5380–5387.
69. Lubitz, W., and Feher, G. (1999) The primary and secondary acceptors in bacterial photosynthesis: III Characterization of the quinone radicals Q<sub>A</sub><sup>-</sup> and Q<sub>B</sub><sup>-</sup> by EPR and ENDOR, *Appl. Magn. Reson.* 17, 1–48.

BI047559M